# Electron kinetics and emission for metal nanoparticles exposed to intense laser pulses

P. Grua, J. P. Morreeuw, and H. Bercegol
*Centre d'Etudes Scientifiques et Techniques d'Aquitaine, Commissariat a l'Energie Atomique, BP No 2 33114 Le Barp, France*

G. Jonusauskas and F. Vallée
*Centre de Physique Moléculaire Optique et Hertzienne, CNRS, Université de Bordeaux I, 351 cours de la Libération, 33405 Talence, France*

(Received 3 December 2002; published 28 July 2003)

A kinetic theory for the interaction of laser radiation with metal nanoparticles embedded in a wide-band-gap dielectric is presented. The formalism is based on the integration of the Boltzmann equation for electrons of an open system, adapted to the description of electron losses from the nanoparticle such as thermionic and photoelectric effects. Differential forms of the electron-electron and electron-phonon collision operators are introduced to perform kinetic calculations beyond the nanosecond time scale. This kinetic model, which also includes nanoparticle-matrix energy transfer, is used to calculate laser energy deposition, redistribution, and electron ejection for nanosecond or picosecond laser-pulse durations in a model system for laser damage investigation; gold nanoparticles embedded in $SiO_2$ glass. Though electron-phonon relaxation times are small compared with laser-pulse duration, an important part of the electron population is found to be driven beyond a typical 10 eV energy. These results suggest that laser absorption by a metal nanoinclusion can create a plasma around the particle.

DOI: 10.1103/PhysRevB.68.035424 PACS number(s): 73.22.−f, 73.63.−b, 73.90.+f, 79.40.+z

## I. INTRODUCTION

Hot electron relaxation dynamics in metal nanoparticles have drawn much attention in the last few years.[1–5] In the scope of femtosecond to picosecond laser-pulse durations, and for low excitation levels, both two-temperature and kinetic formalisms were used to describe the electron ($e$) and phonon ($p$) systems of metals. The main purpose of the above-mentioned experimental and theoretical studies has been the analysis of optical responses of metal nanoparticles, both for understanding their fundamental electronic and vibrational properties and for developing new materials. More recently, another application field for nanoparticle-glass systems has been looked through; the study of laser damage initiation of optical materials,[6–8] using metal nanoparticles as model nanoabsorbing centers.

In laser damage investigation, one is interested in interaction of a high fluence (few J/cm$^2$) laser pulse with the metal nanoparticles. The previous electron kinetics modeling developed in femtosecond or picosecond regimes and for a low fluence are then inadequate. New approaches, including new effects, have to be developed to describe this highly nonlinear regime. For instance, Papernov and Schmid's results show that the energy deposited by the laser pulse inside the metal particle only is not sufficient to produce the observed damage sites.[6,7] In particular, the creation of an electron plasma around the inclusions can modify the absorbing properties of the system (nanoparticle and glass) and be a precursor mechanism to damage. The aim of this paper is to describe the first phase of this process, that is, nanoparticle electron heating and kinetics in a very strong excitation regime, and creation of an electron plasma in the glass, as a result of gold nanoparticle interaction with a high intensity picosecond or nanosecond laser pulse.

The simplest model one can use to describe laser-nanoparticle interaction consists in calculating the absorption of an inclusion through Mie's theory,[9,10] knowing the metal dielectric function. Then, it is possible to determine the evolution of electron and phonon temperatures in metal, as well as in the glass matrix.[1,11] A metallic nanoparticle embedded in glass constitutes a potential well for the metal conduction electrons. The finite depth of this potential well implies that electrons, with energy above a critical value, are able to escape from the inclusion. When this process becomes effective, requiring an electron temperature of order of the electron volt, the temperature concept itself dies out since the electron distribution function can no longer be identified to the Fermi-Dirac function. Hence, explicit calculations for the evolution of the electron distribution function have to be performed using the Boltzmann equation,[12] including increased $e$-$p$ coupling due to $d$-states contribution for large electron heating,[13] nanoparticle-glass energy transfer by electron ejection, and heat diffusion in the matrix.

Such kinetic calculations have drawn much attention in the last few years in the frame of ultrashort pulses. In the case of nanosecond pulses, a major inconvenience is encountered; the resolution of kinetic equations in their integrodifferential form is very computer time consuming. The calculation time can be drastically reduced using a purely differential kinetic equation, allowing implicit numerical integration schemes. We show that it is possible by transforming $e$-$e$ and $e$-$p$ collision operators by the use of Landau diffusion approximations,[14] making these calculations tractable on a standard computer. The fully kinetic model presented in this paper, allows us to determine the amount of ejected electrons from gold nanoinclusions by thermionic emission[15] and photoelectric effect,[16] as a function of particle's dimension and of duration and fluence of the incident laser pulse.

General properties of gold nanoparticles embedded in

 

silica and processes of electron ejection from an inclusion towards the conduction band of silica are summarized in Sec. II. Section III is devoted to the kinetic model describing the metal conduction electrons. In the same section, the method of integration of the Boltzmann equation is detailed. Numerical calculations, modeling laser-nanoparticle interaction with high intensity picosecond and nanosecond pulses in the UV (351 nm), are presented in Sec. IV.

## II. NONTHERMAL EQUILIBRIUM PROCESSES

The system studied is a spherical inclusion of radius $a$ illuminated by a plane and monochromatic laser wave. We shall consider throughout this paper that laser energy deposition is dominated by linear absorption. This constraint will be satisfied for gold nanoparticles if the intensity of the laser pulse, in the wavelength range from 250 nm to 1 $\mu$m, remains approximately below 1 TW/cm$^2$.[17] Using a linear approach on the basis of Mie's theory,[9] and knowing the dielectric function of gold nanoparticle, the determination of the number of photons absorbed per unit time can be performed through an absorption cross section.[11,18] The aim of Sec. II A is to estimate the temperatures reached in glass-nanoparticle systems, and point out the main characteristics of relevant processes. This is achieved on the basis of the two-temperature model[1–4] used to describe the metal dynamics. In Sec. II B, the energy-band structure at the interface between gold nanoparticle and silica is examined, and ejection-recombination process of hot electrons is discussed.

### A. Two-temperature model of the metal and energy exchange with glass

The heating of the whole system can be divided in several stages. Laser energy is first deposited on metal conduction electrons. An electron, which absorbs a photon, will redistribute the corresponding energy on the whole electron population by means of $e$-$e$ collisions, and simultaneously $e$-$p$ collisions will contribute to the gold crystal lattice heating. The glass matrix around the inclusion is in turn heated by thermal diffusion. The two-temperature model, extensively used in the literature,[1–4] can be applied to nanoparticle-glass systems as long as the heating laser pulse is not too short (greater than a few hundred femtoseconds[4,5]), and if the fluence is not too high, in order to keep nonthermal processes negligible, such as energy losses due to electron escape. Hence, the metal is described as a couple of subsystems, an electron system and a phonon system. Each system is assumed to be in local equilibrium and is characterized by its temperature, that is, the electron temperature $T_e$ and the lattice temperature $T_l$. In the case of nanoparticle, the energy transfer between the metal and the glass is a very efficient process. An equation describing the evolution of the glass temperature $T_g$ around the nanoparticle has thus to be added to the two-temperature model. This energy transfer will be assumed to occur through phonon-phonon coupling only.

As it will be shown below, in the frame of this two-temperature approach, a very precise evaluation of the rates of energy exchange between electrons and phonons or through the metal-glass interface is unnecessary. In particular, the influence of the particle size on the rate of $e$-$p$ energy exchange is neglected.[5,19] The time evolutions of the temperatures are obtained with the following coupled heat equations:

$$C_e(T_e)\frac{\partial T_e}{\partial t} = -G(T_e - T_l) + S(t), \tag{1}$$

$$C_l \frac{\partial T_l}{\partial t} = G(T_e - T_l) + S_{lg}, \tag{2}$$

$$C_g \frac{\partial T_g}{\partial t} = \nabla \cdot \kappa_g \nabla T_g, \tag{3}$$

where $C_e$, $C_l$, and $C_g$ reflect electronic, lattice, and glass heat capacities, $G$ is the $e$-$p$ coupling constant, $\kappa_g$ is the glass thermal conductivity, $S(t)$ is the direct heat input to the electron system by the laser pulse, and $S_{lg}$ is the metal-glass energy exchange. The electron and phonon temperatures are assumed to be homogeneous inside the particle and $T_g$ position dependent. The whole system is assumed to present spherical symmetry. As boundary conditions, the phonon temperatures and heat flux are set continuous at metal-glass interface. In this configuration, $S_{lg}$ is given by

$$S_{lg} = 3\frac{\kappa_g}{a}\left(\frac{\partial T_g}{\partial r}\right)_{r=a}, \tag{4}$$

where $a$ is the particle radius. The energy deposition term in Eq. (1) is expressed as

$$S(t) = \frac{\sigma_{abs}}{\frac{4}{3}\pi a^3} I_0(t). \tag{5}$$

Here $I_0$ being the laser intensity and $\sigma_{abs}$ the absorption cross section of the nanoparticle given by[18]

$$\sigma_{abs} = 12\pi a^3 \frac{\omega}{c} \frac{n_0^3 \varepsilon''}{(\varepsilon' + 2n_0^2)^2 + \varepsilon''^2}, \tag{6}$$

where $\omega$ is the laser angular frequency, $c$ is the vacuum light velocity, and $n_0$ is the glass index. The relative dielectric constant of the particle $\varepsilon = \varepsilon' + i\varepsilon''$ takes into account two mechanisms of laser energy deposition in gold: intraband absorption (in the $sp$ band) and interband absorption ($d$ towards $sp$ band).[20] Intraband absorption is described through a Drude model, including effects related to electron mean-free-path limitations,[21] while a Lindhard type model is used for interband contribution.[12,16] Parameters involved in these models are adjusted in order to match the optical properties of the bulk metal in the limit of large particles. For gold nanoparticles embedded in silica and for a laser wavelength $\lambda = 351$ nm, $\sigma_{abs}$ is roughly given by $\sigma_{abs}/(\pi a^2) \approx 0.1a$ nm.

For laser-pulse durations $\tau_{las}$ above 1 ps, the electron temperature can be considered to evolve simultaneously with the intensity of the incident wave. Let us compare the characteristic evolution time of electron temperature resulting from energy deposition with the time of energy exchange

between the nanoparticle and the glass matrix. This energy exchange time is equivalent to the diffusion time of temperature in glass, that is, $a^2 C_g/\kappa_g$, which is in the picosecond range ($C_g=0.163\times10^7$ J/m$^3$/K and $\kappa_g=1.37$ W/m/K for fused silica[22]). Since this time is very small compared with laser-pulse durations we are interested in, the heat flux in glass can be considered to be quasistationary in the neighborhood of the particle. Thus, we have $T_g(r)\approx T_0+(T_l-T_0)\,a/r$ ($T_0$ is the glass temperature for $r\to\infty$), and $S_{lg}$ can be expressed as

$$S_{lg}\approx -3\frac{\kappa_g}{a^2}(T_l-T_0). \tag{7}$$

From Eq. (7), a characteristic time of energy exchange between the nanoparticle and the glass matrix can be properly defined as

$$\tau_m=\frac{a^2 C_l}{3\,\kappa_g}\approx 0.6\,a^2(\mathrm{nm})^2\ \mathrm{ps}. \tag{8}$$

Even for a high-electron temperature ($T_e\sim1$ eV), the lattice specific heat is large compared with electron one ($C_l=2.49\times10^6$ J/m$^3$/K,[22] $C_e\approx\gamma T_e$, $\gamma=63$ J/m$^3$/K$^2$). Hence, neglecting the electron specific heat term with respect to the two-temperature model, and since for nanoparticles we have $\tau_m\ll\tau_{las}$, it is relevant to look for a stationnary solution of the heat equations [Eqs. (1)–(3)]. One obtains

$$T_l(t)\approx T_0+\frac{a^2 S(t)}{3\kappa_g}, \tag{9}$$

$$T_e(t)\approx T_l(t)+\frac{S(t)}{G}. \tag{10}$$

The energy exchange rate between electrons and lattice depends directly on the *e*-*p* coupling constant *G*. We take $G=2.5\times10^{16}$ W/m$^3$/K,[5,23] more precise explanations about this choice are given in Sec. III E. Therefore, if the particle size is of the order of a nanometer, energy loss from the inclusion towards the glass matrix by thermal diffusion is a process more efficient than heating of the gold crystal lattice by *e*-*p* energy exchange. The consequence is that even for a nanosecond-GW/cm$^2$ laser pulse, the phonon temperature $T_l$ can remain rather low, i.e., under the metal melting temperature. For a gold nanoparticle of radius $a=2$ nm and a laser intensity $I_0=0.5$ GW/cm$^2$, one obtains $T_e\approx16\,000$ K and $T_l\approx670$ K.

### B. Electron ejection processes

Two electron ejection processes from a metal towards vacuum are known: the photoelectric effect and thermionic emission. At ambient electron temperature, the photoelectric effect is efficient if the photon energy of incident light is larger than the so-called work function value *W* of the metal (extraction energy from Fermi level). For polycrystalline gold in vacuum, we have $W=5.1$ eV.[22] The nanoparticles may as well be single crystalline and exhibit faces corresponding to low-index planes. In this case, since the work function is different for different planes, it may happen that the electron emission is anisotropic. However, the work functions of single crystalline gold associated with low-index planes present slight differences with respect to the work function of gold in polycrystalline form, below 8%.[22] Hence, in numerical calculations, we will use the work function of polycrystalline gold. For highly excited electron distributions, absorption of 351-nm light (3.53-eV photons) can lead to photoemission of hot electrons. This mechanism can occur through the Drude absorption and inter *s*-*p* band transitions.[24] The respective weights of these two processes can be roughly estimated, first noting that for a nanoparticle, because of mean-free-path limitations effects, the Drude absorption is strongly enhanced with respect to massive material. For 3.53-eV photons, it represents typically 20% of the whole absorption in a nanoparticle (less than 1% in massive material). The partial joint densities of states taken in Ref. 24 corresponding to transitions from the two upper *d* bands towards *p* band, and from *p* towards *s* band, can be used to build the imaginary part of the dielectric function. A comparison of the calculated and experimental[22] dielectric functions permits us to estimate the inter *s*-*p* band transitions efficiency. The results indicate that photoemission induced by this process is negligible as compared to the one related with Drude absorption in gold nanoparticles.

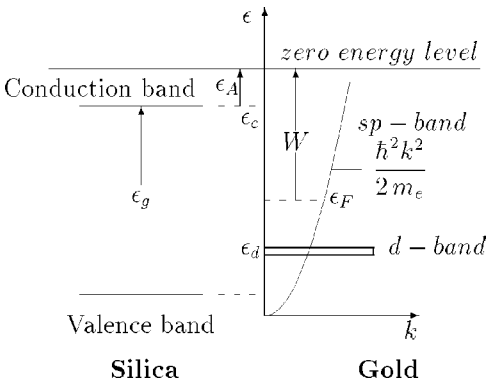


FIG. 1. Diagram of the energy relations at the Au-$SiO_2$ interface.

Electrons can be ejected by thermionic effect if the occupation number around the energy $\epsilon\approx\epsilon_F+W$ is significant. In this case, the electrons close to this threshold can get energy by collision and escape from the metal.

As the metallic particle is embedded in a glass, electrons can be ejected if their energy is sufficient to reach the conduction band of the glass. If we consider electrons at thermodynamic equilibrium, the Fermi levels are identical in the inclusion and in the glass near the interface. In a glass, the location of the Fermi level is not well known, but it is usually located approximately halfway between the top of valence band and the bottom of conduction band.[25] Hence, energies will be referenced with respect to vacuum. As the electron affinity of silica is $\epsilon_A\approx1.2$ eV,[26] the effective work function for the gold-silica interface will be reduced to $W_{eff}=W-\epsilon_A\approx3.9$ eV (Fig. 1). That interfacial barrier height is in an agreement with the values used in studies related to ballistic electron transport in thin $SiO_2$ films.[27]

Since for gold the Fermi energy is $\epsilon_F = 5.53$ eV (with respect to the bottom of parabolic conduction band), we can write the critical ejection energy $\epsilon_c$ as

$$\epsilon_c \approx \epsilon_F + W_{eff} \approx 9.43 \text{ eV}. \tag{11}$$

Electron ejection results in the creation of a positively charged nanoparticle, and hence of strong electrostatic field, which tends to preserve the system quasineutrality. As the silica band gap is $\approx \epsilon_g \approx 8-9$ eV, under the action of the electrostatic field, electrons from the valence band of silica can replace electrons ejected from gold (Fig. 1). This mechanism occurs only if unoccupied electron states in gold are available at the corresponding energies, as this is the case for strong electron heating ($T_e > 3000$ K). Moreover, when the nanoparticle becomes positively charged, the potential energy of the remaining electrons shifts downward, hence the top of the silica valence band can match the energy levels of free electron states in gold. In this recombination scheme, electrons from the valence band of glass fill in the negative charge deficit within the metal particle without having to lose energy. It is thus more likely than recombination with hot electrons in conduction band of glass which involve large energy losses. In such a process, electron emission leads to the formation of electron-hole pairs in glass, which can subsequently form excitons and self-trapped excitons (STE) by losing energy through *e-p* collisions.[28]

## III. KINETIC MODEL

Evaluation of thermionic emission requires the precise knowledge of the distribution tail, at the neighborhood of critical energy $\epsilon_c$. This cannot be done using the above two-temperature model that assumed the electron temperature to be defined. We shall use here a description of the electron kinetics, by its time-dependent distribution function $f(\epsilon)$, assumed to be homogeneous and isotropic, mainly because of the randomization due to the limitation of electron mean free path to particle size. Its evolution is described with the help of the Boltzmann equation that replaces the $T_e$ evolution equation (1) in the two-temperature model. It includes *e-e* and *e-p* collisions, and laser energy deposition through intraband and interband absorption mechanisms:

$$\frac{\partial f(\epsilon)}{\partial t} = \underbrace{\left(\frac{\partial f(\epsilon)}{\partial t}\right)_{intra} + \left(\frac{\partial f(\epsilon)}{\partial t}\right)_{inter}}_{\text{energy deposition}} + \underbrace{\left(\frac{\partial f(\epsilon)}{\partial t}\right)_{e-p} + \left(\frac{\partial f(\epsilon)}{\partial t}\right)_{e-e}}_{\text{energy redistribution}}. \tag{12}$$

This equation reduces to Eq. (1) in the thermal regime.

Linear interband absorption is possible only for laser photons having an energy greater than the *sp-d* band gap, that is, $\epsilon_F - \epsilon_d = 2.45$ eV (Fig. 1). As before, the metal lattice and silica matrix will be described by their temperatures $T_l$ and $T_g$, respectively, using standard heat equations

$$C_l \frac{\partial T_l}{\partial t} = -A \int_0^{\epsilon_c} \left(\frac{\partial f(\epsilon)}{\partial t}\right)_{e\text{-}p} \epsilon^{3/2} d\epsilon + S_{lg} \tag{13}$$

and

$$C_g \frac{\partial T_g}{\partial t} = \nabla(\kappa_g \nabla T_g). \tag{14}$$

The first term of right-hand side of Eq. (13) represents *e-p* energy exchange for a parabolic conduction band of gold. The constant *A*, related to the density of states in conduction band, is written as

$$A = \frac{(2\, m_e)^{3/2}}{2\pi^2 \hbar^3} = \frac{3}{2} \frac{n_e}{\epsilon_F^{3/2}}, \tag{15}$$

where $n_e$ is the electron density in the conduction band.

Expressions of the four operators in Eq. (12) can be found in the literature.[12,17] The energy deposition operators, i.e., the intraband and interband absorption operators $(\partial f(\epsilon)/\partial t)_{intra}$ and $(\partial f(\epsilon)/\partial t)_{inter}$ are detailed in the Appendix. They can be easily numerically evaluated. On the other hand, if energy redistribution operators are expressed in their canonical form, they involve the evaluation of single integrals for *e-p* collisions and double integrals for *e-e* collisions, in each point of phase space.[4,12,29,30] In practice, these types of calculations are feasible only in the case of an extremely short phenomena, corresponding to the ultrashort laser-pulse physics, in the femtosecond range. A numerical calculation performed using an *e-e* collision operator in its integral form typically requires a computation time of 1 h/ps, that is 40 days/ns on a standard main frame computer (for example, an IBM-SP2). In order to model the phenomena of much longer duration, the use of the collision operators in their standard forms is not always necessary. This form is fully justified only if distribution functions differ in a significant way from the Fermi-Dirac function. The fact that *e-e* and *e-p* relaxation times are typically of the order of a few tens of femtoseconds, means that above the picosecond range, a kinetic calculation consists in looking for an electron distribution function near equilibrium. Hence, we can approximate integral operators to differential operators. This latter form evidently avoids the calculation of integrals, but moreover allows the use of implicit numerical schemes and suppresses mesh constraints inherent in integral formulations. This procedure saves computation time by a factor $10^4$.

### A. Electron-phonon collision operator, integral, and differential forms

The transformation of *e-p* collision operator is first detailed on the basis of the operator adapted to low electron temperatures ($T_e < 3000$ K), which leads to satisfactory results in this temperature range. We give below the necessary adjustments in the case of high electron temperatures, up to 1 eV (Sec. III E).

#### *1. Integral form*

The integral *e-p* collision operator for acoustic phonons is written in the deformation potential approximation[29] as

$$\left(\frac{\partial f(\epsilon)}{\partial t}\right)_{e-p} = K_{ep}\int_0^{q_D}\frac{q^2}{\sqrt{\epsilon}}dq\, C(f,N) \tag{16}$$

with

$$\begin{aligned} C(f,N) = {} & f(\epsilon-u)[1-f(\epsilon)]N_u - f(\epsilon)[1-f(\epsilon-u)](1+N_u) \\ & + f(\epsilon+u)[1-f(\epsilon)](1+N_u) \\ & - f(\epsilon)[1-f(\epsilon+u)]N_u, \end{aligned}$$

where $f$ is the electron distribution function and $N$ is the phonon one; $\epsilon$ and $u$ are electron and phonon energies, respectively. $q$ represents the phonon wave number and $q_D$ the Debye wave number, expressed as a function of interatomic distance $d$: $q_D=(3/4\pi)^{1/3}2\pi/d$. The phonon energy is related to their wave number by $u=\hbar\, c_s\, q$, where $c_s$ is the sound velocity. The $K_{ep}$ constant is given by

$$K_{ep}=\frac{2^{3/2}\pi^2\hbar^3 G}{m_e^{3/2}k_B T_D q_D^3}, \tag{17}$$

where $G$ is the *e-p* coupling constant and $T_D$ is the Debye temperature $[k_B T_D = u(q_D) = \hbar\, c_s\, q_D]$.

#### *2. Differential form*

Since the electron energy is typically large with respect to phonon one ($u\sim 10$ meV, $\epsilon\sim 1$ eV), it is possible to make use of Landau approximation,[14] which allows us to express the collision operator in a differential form. For this, we perform a Taylor expansion of $C(f,N)$ function, up to second order with respect to the small parameter $u$. Straightforward calculations give

$$C(f,N)\approx u\frac{\partial}{\partial\epsilon}(f(\epsilon)[1-f(\epsilon)])+(1+2N_u)\frac{u^2}{2}\frac{\partial^2 f(\epsilon)}{\partial\epsilon^2}.$$

We consider phonons to be in thermal equilibrium, at a temperature $T_l$. In this case $N_u$ is the Bose-Einstein function, and if the crystal lattice temperature is above the Debye temperature (that is always verified for noble metals at ambient temperature), one easily checks that $1+2N_u\approx 2k_B T_l/u$. The $C(f,N)$ function is then written as

$$C(f,N)\approx u\frac{\partial}{\partial\epsilon}\left(f(\epsilon)[1-f(\epsilon)]+k_B T_l\frac{\partial f(\epsilon)}{\partial\epsilon}\right). \tag{18}$$

Performing the explicit integration with respect to $u$ in Eq. (16), we obtain the *e-p* collision operator in its differential form

$$\left(\frac{\partial f(\epsilon)}{\partial t}\right)_{e-p}=\frac{C_{ep}}{\sqrt{\epsilon}}\frac{\partial}{\partial\epsilon}\left(f(\epsilon)[1-f(\epsilon)]+k_B T_l\frac{\partial f(\epsilon)}{\partial\epsilon}\right) \tag{19}$$

with $C_{ep}=\pi^2\hbar^3 G/\sqrt{2}k_B m_e^{3/2}$.

### B. Electron-electron collision operator, integral and differential forms

#### *1. Integral form*

The transitions which occur in *e-e* collisions are of the type $e_\epsilon + e_{\epsilon_1}\rightarrow e_{\epsilon_2}+e_{\epsilon_3}$, where total energy and momentum are conserved. The transition matrix elements are calculated using an interaction Hamiltonian related to Coulomb potential energy of electrons, taking into account screening through a Thomas-Fermi dielectric function.[16] Neglecting the exchange terms, the operator reads[30] as

$$\left(\frac{\partial f(\epsilon)}{\partial t}\right)_{e-e}=\frac{K_{ee}}{\epsilon_s^{3/2}\sqrt{\epsilon}}\int d\epsilon_1\int d\epsilon_2\, F(\epsilon,\epsilon_1,\epsilon_2) \times\left[\frac{\sqrt{x}}{1+x}+\arctan\sqrt{x}\right]_{x_{min}}^{x_{max}}, \tag{20}$$

with $K_{ee}=m_e e^4/(4h^3\varepsilon^2)$, $\varepsilon$ being the electrostatic approximation of permittivity,[16] and the energy $\epsilon_s$, defined on the basis of Thomas-Fermi wave number $q_s$, is given by

$$\epsilon_s=\frac{\hbar^2 q_s^2}{2m_e}=\frac{e^2}{2\pi\varepsilon}\left(\frac{3n_e}{\pi}\right)^{1/3}.$$

Pauli's exclusion principle is represented by the function $F$. With $\epsilon_3=\epsilon+\epsilon_1-\epsilon_2$, we have

$$\begin{aligned} F(\epsilon,\epsilon_1,\epsilon_2) = {} & [1-f(\epsilon)][1-f(\epsilon_1)]f(\epsilon_2)f(\epsilon_3) \\ & - f(\epsilon)f(\epsilon_1)[1-f(\epsilon_2)][1-f(\epsilon_3)], \end{aligned}$$

and the integration bounds are

$$x_{min}=\frac{\max((\sqrt{\epsilon_1}-\sqrt{\epsilon_3})^2,(\sqrt{\epsilon}-\sqrt{\epsilon_2})^2)}{\epsilon_s},$$

$$x_{max}=\frac{\min((\sqrt{\epsilon_1}+\sqrt{\epsilon_3})^2,(\sqrt{\epsilon}+\sqrt{\epsilon_2})^2)}{\epsilon_s}.$$

#### *2. Differential form*

In the case of *e-p* collision operator, the maximum energy exchange by an electron with phonon population was limited to the maximum energy of phonons. This quantity could be considered as a small parameter, and the conditions of applicability of Landau approximation were fulfilled. This is not the case for the *e-e* collision operator, Landau approximation is not straightforwardly usable. Because of strong screening in a metal (the characteristic screening distance is of the order of the crystal lattice mesh), *e-e* collisions are of the ''hard spheres'' type. During a single collision, energy exchange can be of the same order as the maximum energy $\epsilon_c$. However, considering the above process as a marginal case, we are able to build an *e-e* operator in differential form, the use of which being accurate as long as the characteristic time of evolution of the distribution function is large compared with the *e-e* collision time. In Sec. III C, the high reliability of the *e-e* differential operator will be demonstrated on the basis of a numerical example. Introducing a self-relaxation

process, the action of this operator will be similar to the one of *e-p* operators. In other words, electron population relaxes on itself, instead of relaxing on different species. First, the operator must satisfy two constraints, the particle number and energy conservations, evidently while this corresponds to a physical reality or if we consider the particular case $\epsilon_c \rightarrow \infty$. These considerations lead to the operator

$$\left(\frac{\partial f(\epsilon)}{\partial t}\right)_{e-e} = \frac{f(0)C_{ee}}{\sqrt{\epsilon}} \frac{\partial}{\partial \epsilon}\left( f(\epsilon)[1-f(\epsilon)] + k_B T_e^* \frac{\partial f(\epsilon)}{\partial \epsilon}\right). \tag{21}$$

$C_{ee}$ is a parameter not explicitly dependent on electron energy, which remains to be evaluated, and $T_e^*$ is the effective electron temperature defined by

$$k_B T_e^* = \frac{1}{f(0)} \int_0^{\epsilon_c} f(w)[1-f(w)]\, dw.$$

This effective temperature is exactly the thermodynamic electron temperature if the distribution function $f$ is the Fermi-Dirac function, and moreover having to verify $f(\epsilon_c) \approx 0$. This is verified as long as $T_e^*$ remains below $\sim 5000$ K. To determine the $C_{ee}$ parameter, we shall proceed on the basis of the analogy with the two-temperature model. It comes as

$$C_{ee} = \alpha_{ee} \frac{\sqrt{2}\, n_e\, h^3}{16\, \pi\, m_e^{3/2} f(0)} \left\langle \frac{1}{\tau_{e-e}} \right\rangle, \tag{22}$$

$$\left\langle \frac{1}{\tau_{e-e}} \right\rangle = \frac{\displaystyle\int_0^{\epsilon_c} \frac{f(w)[1-f(w)]}{\tau_{e-e}(w)} dw}{\displaystyle\int_0^{\epsilon_c} f(w)[1-f(w)] dw},$$

the collision frequency being calculated using the *e-e* collision operator (20), and $\alpha_{ee}$ is an adjusting coefficient of the order of unity, evaluated using the identification of second-order energy momenta.

### C. Test of electron-electron collision operator

The test of the *e-e* collision operator in its differential form has a main goal; showing its applicability to the process of electron ejection. Physically, this test corresponds to the cooling of a hot electron population, which occurs while the system loses high-energy electrons from the distribution tail. Hence, we shall calculate the electron-density change in a nanoparticle, considering that emitted electrons are not replaced, without taking into account electrostatic effects. The test is built in the following way.

(1) The initial distribution function is the Fermi-Dirac function: $f(\epsilon) = 1/(1+\exp[\epsilon-\mu(T_e)]/k_B T_e)$, where $\mu$ is the chemical potential and $T_e = 1$ eV; the function is modified around $\epsilon = \epsilon_c$ in order to match the condition $f(\epsilon_c) = 0$, and having chosen $\epsilon_c = 2\ \epsilon_F$

(2) The evolution of the distribution function is controlled only by *e-e* collision operator

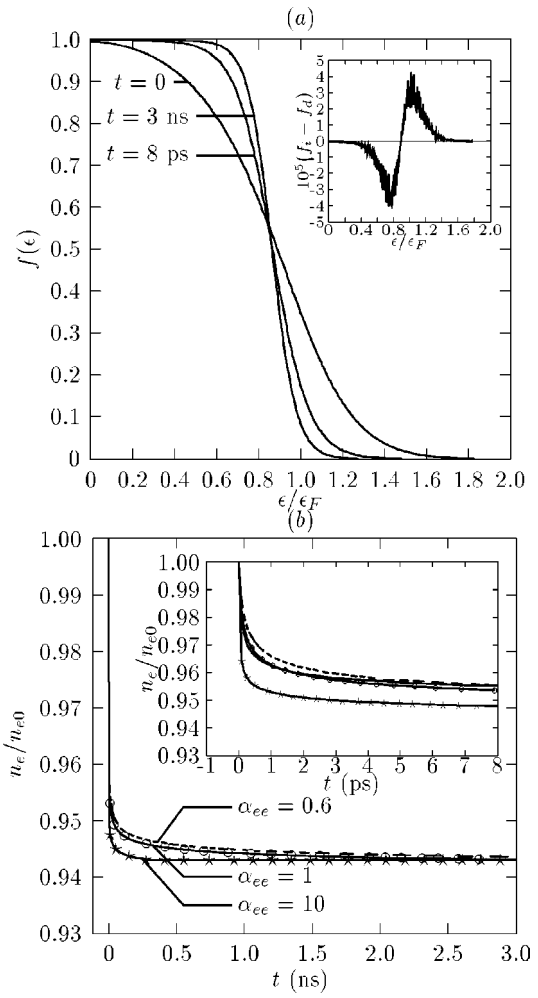


FIG. 2. Distribution function for $t = 0$, 8 ps, and 3 ns (a), the absolute difference between distribution functions calculated using the differential operator ($f_d$) with $\alpha_{ee} = 0.6$ and the integral operator ($f_i$) at $t = 8$ ps is reported in the inset; evolution of the electron density during 3 ns for three values of the $\alpha_{ee}$ coefficient (b). Inset shows the density variation during the first picoseconds, the solid line corresponding to exact calculation.

(3) Calculations are realized using the differential operator on a 3 ns duration and the integral operator on a 8 ps duration.

(4) Three values of the adjusting coefficient $\alpha_{ee}$ are used to perform calculations in differential forms.

We expect the system to evolve towards a stationary configuration having lost one part of its electrons. The amount of lost electrons must be the same for every $\alpha_{ee}$ value, which must only have an influence on the delay to reach the equilibrium state. Results obtained using the differential form of the operator are compared with those obtained using the integral form in the picosecond range. The evolution of the distribution function is shown at times $t = 0$, 8 ps, and 3 ns [Fig. 2(a)]. For $t = 8$ ps, results arising from integral and differential operators with $\alpha_{ee} = 0.6$ are practically identical [inset of Fig. 2(a)]. At $t = 3$ ns, the system has lost nearly 5% of its electrons [Fig. 2(b)], the associated energy loss leads to a decrease of the effective temperature. One can verify that the

choice of $\alpha_{ee}$ coefficient has a little influence on the ejection rate in nanosecond range, and in every case the system evolves towards the same stationary state. Moreover, the main part of the electron ejection process takes place during the first few picoseconds [inset of Fig. 2(b)].

Fixed values of the $\alpha_{ee}$ coefficient were used in order to point out their little influence on final results. Of course, in realistic calculations, $\alpha_{ee}$ will be adjusted by the procedure of identification of second-order energy momenta. Therefore, we can conclude that our *e-e* collisions operator in differential form describes accurately the evolution of the distribution function, as well as related processes.

### D. Rates of electron ejection

#### 1. Photoelectric effect

The laser energy deposition involves intraband and interband absorption mechanisms. We shall consider that the photon energies are below 5 eV. In this case, only the intraband mechanism is able to contribute directly to electron ejection, since the interband mechanism corresponds to transitions from an energy level $\epsilon_d$ towards an energy $\epsilon_d+\hbar\omega$, well below the critical ejection energy $\epsilon_c$. The change of electron density due to photoelectric effect is written with the help of the intraband absorption operator [Eq. (A1) in the Appendix] as

$$\left(\frac{\partial n_e}{\partial t}\right)_{ph} = A\int_0^{\epsilon_c}\left(\frac{\partial f}{\partial t}\right)_{intra}\sqrt{\epsilon}\,d\epsilon, \tag{23}$$

that is,

$$\left(\frac{\partial n_e}{\partial t}\right)_{ph} = -A\,K_{intra}\int_{\epsilon_c-\hbar\omega}^{\epsilon_c} f(\epsilon)\sqrt{\epsilon(\epsilon+\hbar\omega)}\,d\epsilon. \tag{24}$$

The associated energy balance yields the energy losses:

$$\left(\frac{\partial n_e\langle\epsilon\rangle}{\partial t}\right)_{ph} = -A\,K_{intra}\int_{\epsilon_c-\hbar\omega}^{\epsilon_c}\epsilon^{3/2}\sqrt{\epsilon+\hbar\omega}f(\epsilon)d\epsilon. \tag{25}$$

#### 2. Thermionic effect

The electrons from distribution tail can be ejected by the thermionic effect. Electron and energy losses associated with thermionic effect are evaluated on the basis of outward fluxes at $\epsilon=\epsilon_c$. According to a relation similar to the one given by Eq. (23), and using this time the operators (19) and (21), one obtains the emission rates due to *e-p* and *e-e* collisions:

$$\left(\frac{\partial n_e}{\partial t}\right)_{th,p} = A\,C_{ep}\,k_B\,T_l\left(\frac{\partial f(\epsilon)}{\partial\epsilon}\right)_{\epsilon=\epsilon_c}, \tag{26}$$

$$\left(\frac{\partial n_e}{\partial t}\right)_{th,e} = A\,C_{ee}\,k_B\,T_e^*\left(\frac{\partial f(\epsilon)}{\partial\epsilon}\right)_{\epsilon=\epsilon_c}. \tag{27}$$

The corresponding energy losses are simply the product of the rates by the energy $\epsilon_c$.

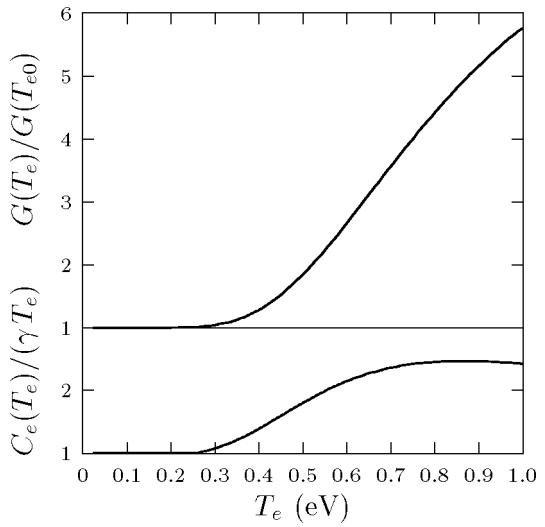


FIG. 3. Enhancement factors of electron-phonon coupling constant and electron specific heat for gold as a function of electron temperature.

### E. Adjustments of physical constants

As electron temperature becomes of the order of electron volt, processes which are negligible at low temperature can become effective, leading mainly to a change of the *e-p* coupling constant $G$ and of the electron specific heat. For instance, Lugovskoy and Bray[17] have made the hypothesis of the contribution of *umklapp* processes. Taking into account these effects can be done by introducing an effective coupling constant $G$, which increases with the electron temperature. Using their model, they have performed simulations of the experiments of Fann *et al.*[23] in thin gold films (30 nm). A very strong coupling constant value at room temperature ($G=2.7\times10^{17}$ W/m$^3$/K) and the usual electron specific heat have been used. However, their estimation of absorbed laser fluence is too high by a factor about 2, leading to an overestimate of temperatures and thus necessitates an enhanced cooling process in such a way to match the experimental results.

On the other hand, Wang *et al.*[13] have included the fact that for high temperatures, the electron density of states which must be considered in the low-energy range is not the one associated with a parabolic conduction band, but a density of states reflecting the existence of the *d* band. Taking into account electron thermal diffusion and the effect related to the density of states towards low energies, a good agreement with experimental results on electron temperature relaxation in gold films, up to $T_e=1$ eV, was obtained. Hence, in our numerical calculations, we have chosen to introduce the determination of the $G$ constant and of the electron specific heat as functions of $T_e$, as given in Ref. 13. The density of states that we have used derives from Ref. 24 and the *e-p* coupling constant at room temperature is $G=2.5\times10^{16}$ W/m$^3$/K. For example, the $G$ constant at $T_e=1$ eV is six times larger than for $T_e=T_{e0}=300$ K and the electron specific heat is increased by a factor about 3 (Fig. 3). It must be noted that the use of our kinetic model to simulate Fann *et al.* experiments yields a very good agreement.[31]

### IV. LASER-NANOPARTICLE INTERACTION

The above approach permits us to model laser-nanoparticle interaction in nanosecond and picosecond pulse ranges, situations corresponding to model systems for laser damage investigations. Such experiments were performed by Papernov and Schmid,[6,7] in $SiO_2$-thin-film doped with gold nanoparticles. The tested samples are 180-nm-thick silica films in which gold nanoparticles were lodged at a depth of 60 nm, with a mean surface density of the order of one particle per $\mu m^2$. To study damage thresholds and morphology, samples were irradiated with 351-nm, 0.5-ns laser pulses. The presence of gold nanoinclusions led to the appearance of craters with the following characteristics: submicrometric with smooth walls (diameter $\sim 0.2\ \mu m$) and absence of fracture or scaling off traces. Their formation was ascribed to heating, melting, and vaporization of the silica initially contained in the crater volume. Numerical estimates based on such considerations suggest that crater formation cannot proceed only through laser energy absorption confined within the particle. It instead starts in the particle and then spreads out to the surrounding matrix during the laser pulse. The electron plasma generated around the inclusion may play this rôle since it would provide a strong enhancement of the absorption of the surrounding silica. The first step of the plasma creation initiated by laser-nanoparticle interaction can be described using our kinetic model.

At this stage, several fundamental questions arise: what is the extent of such an electron plasma and which physical mechanisms may induce absorption coefficient changes ? Whereas in fused silica, the dynamics of electron-hole pairs created by femtosecond laser pulses at room temperature is quite well understood,[28,32,33] the case of nongemellar electron-hole pairs[34] or of silica at high temperatures up to the melting point still require some more investigations. However, since electron-hole pairs are believed to lead to a very fast ($\sim 150$ fs) creation of STE's up to very high densities (approximately the $SiO_2$ sites density of $2 \times 10^{22}\ cm^{-3}$),[28,35] as a first approximation, the electron and hole transport in silica can be neglected provided that the number of emitted electrons does not exceed the number of $SiO_2$ sites contained in a few shells around the nanoparticle. Hence, this critical value can be set to the number of conduction electrons of the nanoparticle. In this frame, our calculations will be representative of damage initiation mechanisms.

The numerical calculations, which are presented, are based on two assumptions: energy is deposited in the gold nanoinclusion only and the emission-recombination process described in section II B has been adopted; that is, each emitted electron at critical point $\epsilon_c$ is instantaneously replaced by an electron from valence band of $SiO_2$. For the nanosecond pulses, the simulations of laser interaction with gold nanoparticles of 1.3 and 2.6 nm radii have beeen performed, as were tested in Papernov and Schmid experiments. In order to show the influence of laser-pulse duration and laser intensity, the calculations corresponding to the same nanoparticles exposed to a 50-ps pulse are also presented. In both cases, the laser wavelength is 351 nm.

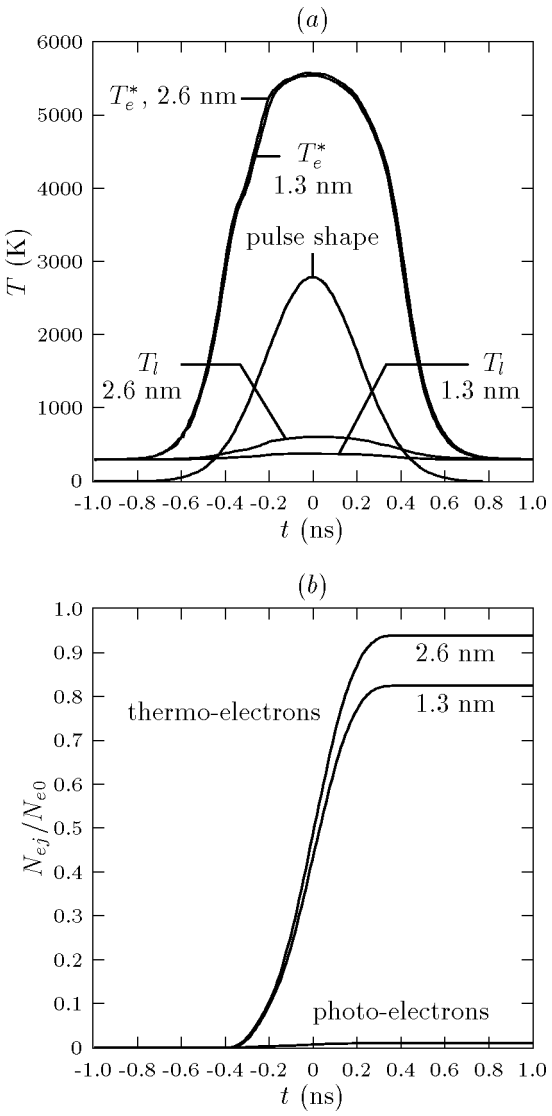


FIG. 4. Gold nanoparticles having 1.3- and 2.6-nm radii, illuminated by a 0.5-ns laser pulse, for a fluence of 0.3 J/cm$^2$: (a) evolution of effective electron temperature and phonon temperature; (b) ratio of the number of ejected electrons by the number of conduction electrons inside the particle ($N_{e0}=540$ for $a=1.3$ nm and $N_{e0}=4300$ for $a=2.6$ nm).

Results of simulations for nanosecond pulses are shown in Figs. 4 and 5, the pulse duration is 0.5 ns and the fluence is 0.3 J/cm$^2$, yielding a maximum laser intensity of $\approx 0.6$ GW/cm$^2$. The effective electron temperatures in the metal saturates well below 1 eV, while the gold crystal lattice temperature reaches 620 K for $a=2.6$ nm and 390 K only for $a=1.3$ nm [Fig. 4(a)], the heat transfer from metal towards glass being more efficient for the smaller particle. A very important remark must be made; the levels of electron temperature in gold nanoinclusions, calculated with a classical two-temperature model, would be more than twice high as the levels obtained with the kinetic model. For example, using Eq. (9) for the 2.6-nm particle, one finds $T_e \approx 15\,000$ K (5600 K read in Fig. 4). The strong difference is due to the changes of thermodynamic properties of the sys-

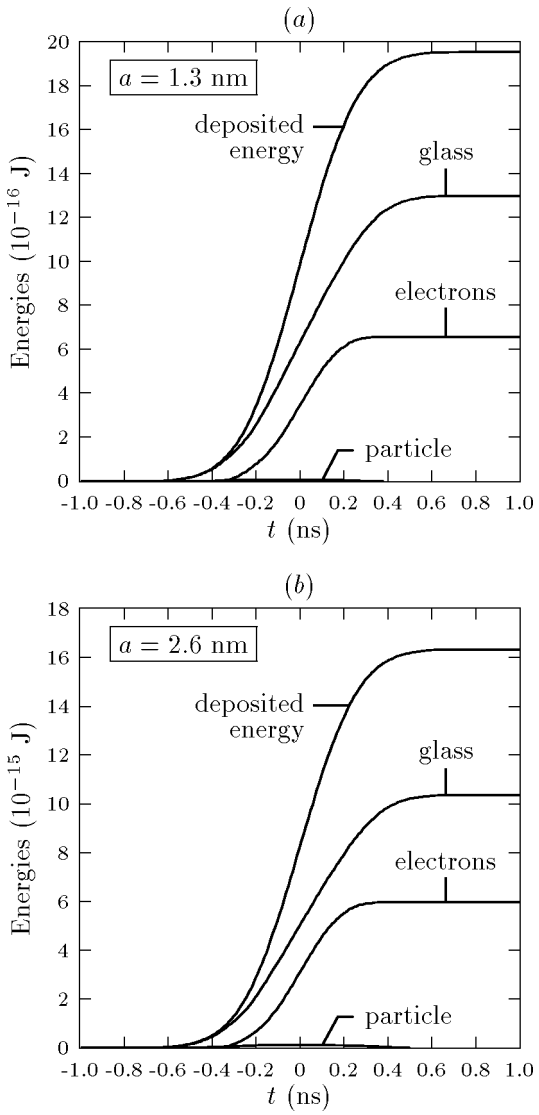


FIG. 5. Energy balance for 1.3- and 2.6-nm particles, relative to configurations of Fig. 4: deposited energy, energy that is taken away by ejected electrons, energy that has been transferred to glass by thermal conduction, and energy stored inside the particle.

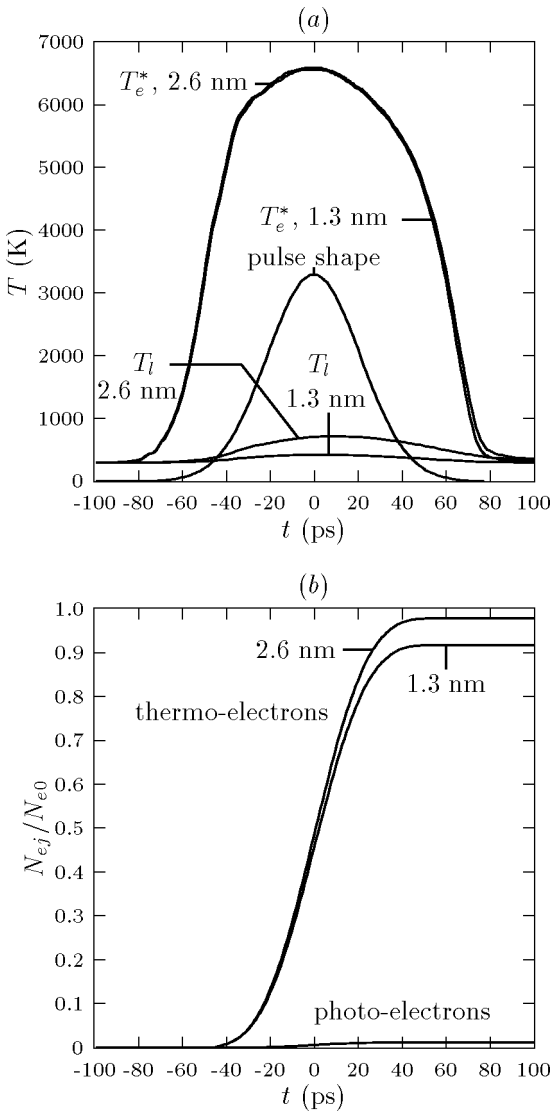


FIG. 6. Same as Fig. 4, but in the picosecond regime: the laser-pulse duration is 50 ps and the fluence is 0.15 J/cm$^2$.

tem with electron temperature, mainly the *e-p* coupling constant, and due to the saturation of the electron energy in the inclusion, related to electron ejection processes. The number of ejected electrons is shown in Fig. 4(b). The thermionic effect is strongly dominant with respect to photoelectric effect. The reason is that for gold at 351 nm, the inter *d-sp* absorption is much more efficient than intraband absorption, which is the dominant mechanism able to induce photoelectric effect for such a photon energy (3.53 eV). One can observe that the ratio of ejected electrons is higher for the 2.6-nm particle. This is due to slightly higher effective electron temperature reached in the larger particle, and to the significant phonon temperature difference since *e-p* collisions act on electron ejection rate [Eq. (26)]. One can note that the major part of the energy, which is deposited in the nanoparticle, has been transferred to glass by thermal conduction (Fig. 5). Another part of the deposited energy is taken away by ejected electrons, and the energy part remaining inside the particle is negligible with respect to other ones.

For the high peak power regime attained with picosecond pulses, we used a pulse duration of 50 ps and a fluence of 0.15 J/cm$^2$ (Figs. 6 and 7); in this case, the maximum laser intensity reaches 3 GW/cm$^2$. This higher intensity leads to a larger transient energy of the electrons and modifies their kinetics as compared to the nanosecond range. It shows up by more pronounced saturation of effective electron temperature as the laser intensity approaches its maximum value [Fig. 6(a)], while the highest ejection rate of electrons is obtained [Fig. 6(b)]. This indicates that electron ejection is the dominant energy loss mechanism in the high peak power regime. It is confirmed by energy balance calculation: the major part of the energy, which is deposited in the nanoparticle, is taken away by ejected electrons rather than transferred to glass by thermal conduction (Fig. 7). Energetic spectrum of the ejected electrons when $T_e^*$ is maximum has been calculated using the integral *e-e* collision operator (Fig.

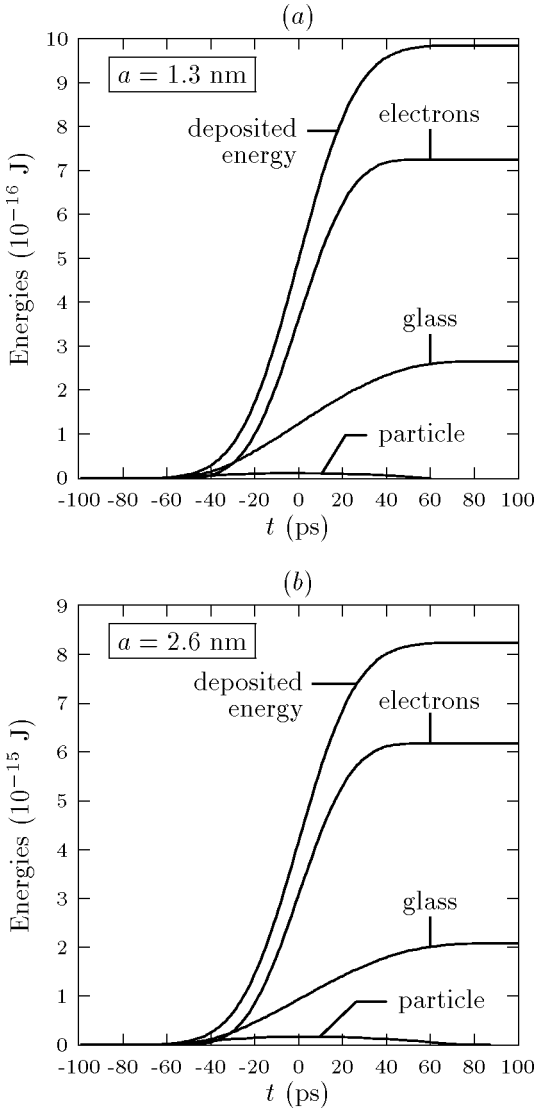


FIG. 7. Energy balance relative to configurations of Fig. 6 in picosecond regime: the energy that is taken away by ejected electrons becomes dominant with respect to the energy transferred to glass by thermal conduction.

8). The maximum kinetic energy of emitted electrons is of the order of the gold Fermi energy, and the spectrum is well fitted by a Maxwellian distribution with an effective temperature of about 1 eV. The knowledge of such an energetic spectrum is necessary to introduce electron transport in silica in further theoretical modeling.

## V. CONCLUSIONS

A kinetic model has been developed to describe the interaction of a strong nanosecond or picosecond laser pulse with a metallic nanoparticle embedded in a glass matrix. Electron-lattice energy exchanges in the metal, energy transfer to the surrounding glass, and electron emission by photoemission and thermionic effects were taken into account. For a strong excitation, electron energy can be larger than the ionization threshold and an electron temperature cannot be defined, precluding modeling by the two-temperature model. The approach is thus based on a detailed description of the energy distribution function kinetics of the metal electrons by the Boltzmann equation, including electron excitation by intraband and interband laser pulse absorption, electron-electron scattering, and electron excitation dependent electron-phonon coupling. The metal lattice and surrounding glass are described by their temperatures, taking into account heat diffusion in the glass.

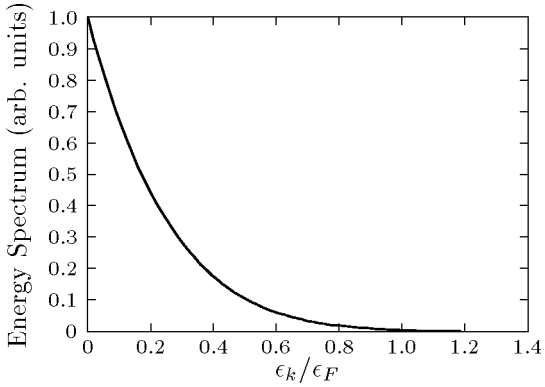


FIG. 8. Energy spectrum of ejected electrons, while $T_e$ is at its maximum (electron kinetic energy $\epsilon_k$ expressed in Fermi energy units $\epsilon_F = 5.53$ eV).

This description required numerical integration of the electron Boltzmann equation over a nanosecond time scale. As it is too computer time consuming to be performed using the usual integral form of the *e-e* and *e-p* collision operators, differential forms have been introduced strongly reducing the computation time. Calculations were performed in the case of gold nanoparticles of 1.3 and 2.6 nm radii in a $SiO_2$ matrix for 0.5-ns pulse at 351 nm and a pump fluence of 0.3 J/cm$^2$, and for 50 ps pulse and 0.15 J/cm$^2$ fluence. In these regimes, we show that a significant number of electrons can be ejected from the nanoinclusion, mainly by thermionic emission. In both cases, the effective electron temperature in a nanoinclusion saturates below typically 1 eV, due to heat transfer to the surrounding glass and ejection of the higher-energy electrons. The latter process dominates for high peak power intensity pulses that create higher nonequilibrium electron distributions.

Electron emission from the metal nanoparticles accompanied by recombination to preserve quasineutrality has been assumed here. It leads to ''pumping'' of the electrons from the valence band of the glass, creating electron-hole pairs and, subsequently, self-trapped excitons. These can modify the material optical properties, and in particular its absorption, and contribute to laser damage initiation in these model systems. Here electron transport in the glass is a key process for further modeling the laser-nanoparticle-glass interactions. Furthermore, electron emission without or with only partial recombination could also take place especially in porous silica samples, for which the metal-glass contact can be poor. Electrostatic effects then become relevant and can eventually induce electrostatic explosion of the inclusions as observed for metal clusters irradiated by an intense laser pulse in vacuum.[36] This aspect of laser-nanoparticle interaction, to-

gether with electron transport in the glass, will be considered in future works.

## APPENDIX: ENERGY DEPOSITION OPERATORS

The energy deposition operators appearing in Eq. (12) make use of transition matrix elements between electron states, which necessitate drastic approximations to be evaluated. As specified above, only linear absorption mechanisms are considered. In this case, operators can be adjusted according to experimental measurements of energy deposition in the gold bulk or in gold nanoinclusions, energy deposition being directly related to the dielectric function of materials. After the determination of functional dependences of operators, it remains a multiplicative constant, which is fixed through energy balance.

### 1. Intraband absorption

Consider first the energy deposition resulting from intraband absorption assisted by phonons. Basically, the fact is that a three-body process requires a virtual state for the electron of the conduction band, which absorbs a photon, and must absorb or emit a phonon in order to reach an allowed state. However, the photon momentum being negligible with respect to the phonon one, and the photon energy being large with respect to phonon energy, the principles of energy and momentum conservation will be expressed in a simplified form, involving explicitly the photon and electron energies only. The occupation number $f(\epsilon)$ can be modified by four mechanisms, the emission/absorption of a photon by electrons leading to transitions between states whose energies are $\epsilon$ and $\epsilon \pm \hbar\omega$, $\hbar\omega$ being the photon energy. The operator is then written as

$$\left(\frac{\partial f(\epsilon)}{\partial t}\right)_{intra} = K_{intra}(F_a^+ + F_e^+ + F_a^- + F_e^-). \quad \text{(A1)}$$

$F_a^+$ is related to the transition probability per unit time corresponding to the absorption of a photon of energy $\hbar\omega$ by an electron of energy $\epsilon - \hbar\omega$. This term is written as

$$F_a^+ = \sqrt{\epsilon - \hbar\omega} f(\epsilon - \hbar\omega)[1 - f(\epsilon)],$$

the square root comes from the density of states around $\epsilon - \hbar\omega$ and $1-f$ from Pauli's exclusion principle. Similarly, we have $F_e^+ = \sqrt{\epsilon + \hbar\omega} f(\epsilon + \hbar\omega)[1 - f(\epsilon)]$, $F_a^- = -\sqrt{\epsilon + \hbar\omega} f(\epsilon)[1 - f(\epsilon + \hbar\omega)]$, and $F_e^- = -\sqrt{\epsilon - \hbar\omega} f(\epsilon)[1 - f(\epsilon - \hbar\omega)]$. The whole energy deposition per unit volume is given by Eq. (5). The dielectric function of gold is related to intraband and interband absorption processes: $\varepsilon = \varepsilon_{intra} + \varepsilon_{inter}$. The Drude term $\varepsilon_{intra}$ takes into account electron mean-free-path limitation effects, and the interband contribution $\varepsilon_{inter}$ is of Lindhard type. Energy deposition can also be written $S(t) = S_{intra}(t) + S_{inter}(t)$, with

$$S_{intra}(t) = \frac{\varepsilon''_{intra}}{\varepsilon''} S(t), \quad \text{(A2)}$$

$$S_{inter}(t) = \frac{\varepsilon''_{inter}}{\varepsilon''} S(t), \quad \text{(A3)}$$

with $\varepsilon'' = \varepsilon''_{intra} + \varepsilon''_{inter}$. Hence, the energy balance for intraband absorption reads as

$$\frac{\partial}{\partial t}\langle n_e \epsilon \rangle_{intra} = S_{intra}(t) = A \int_0^{\epsilon_c} \left(\frac{\partial f(\epsilon)}{\partial t}\right)_{intra} \epsilon^{3/2} d\epsilon, \quad \text{(A4)}$$

allowing to deduce the $K_{intra}$ parameter

$$K_{intra} = \frac{S_{intra}}{A\hbar\omega(I_1 + I_2)}, \quad \text{(A5)}$$

with

$$I_1 = \int_0^{\epsilon_c - \hbar\omega} \sqrt{\epsilon(\epsilon + \hbar\omega)}[f(\epsilon) - f(\epsilon + \hbar\omega)] d\epsilon, \quad \text{(A6)}$$

$$I_2 = \int_{\epsilon_c - \hbar\omega}^{\epsilon_c} \sqrt{\epsilon(\epsilon + \hbar\omega)} f(\epsilon) d\epsilon. \quad \text{(A7)}$$

### 2. Interband absorption

Let us split the interband absorption operator in two parts, each of these parts increasing or reducing the occupation number for a given energy:

$$\left(\frac{\partial f(\epsilon)}{\partial t}\right)_{inter} = \left(\frac{\partial f(\epsilon)}{\partial t}\right)_{inter}^{+} + \left(\frac{\partial f(\epsilon)}{\partial t}\right)_{inter}^{-}.$$

Neglecting the *d*-band dispersion (Fig. 1), the first part of the operator takes the form

$$\left(\frac{\partial f(\epsilon)}{\partial t}\right)_{inter}^{+} = K_{inter}^{+}[1 - f(\epsilon)]\delta(\epsilon - \epsilon_f), \quad \text{(A8)}$$

where $\epsilon_f = \epsilon_F + \hbar(\omega - \omega_g)$, $\delta$ is the Dirac distribution, and $\hbar\omega_g$ is the energy gap between *d* band and Fermi level. Assuming that the electron transition probability from *sp* band towards *d* band is proportional to the occupation number in *sp* band, the second part of the operator is written as

$$\left(\frac{\partial f(\epsilon)}{\partial t}\right)_{inter}^{-} = K_{inter}^{-} f(\epsilon)[1 - \mathcal{H}(\epsilon - \epsilon_f)],$$

where $\mathcal{H}$ is the Heaviside distribution. Each part of the operator gives rise to an electron density change in *sp* band given by

$$\left(\frac{\partial n_e}{\partial t}\right)_{inter}^{\pm} = A \int_0^{\epsilon_c} \left(\frac{\partial f(\epsilon)}{\partial t}\right)_{inter}^{\pm} \sqrt{\epsilon}\, d\epsilon,$$

which permits to obtain the following relation between $K_{inter}^{+}$ and $K_{inter}^{-}$ parameters:

$$K_{inter}^{-}=K_{inter}^{+}\frac{\sqrt{\epsilon_f}[1-f(\epsilon_f)]}{\int_0^{\epsilon_f}\sqrt{\epsilon}f(\epsilon)d\epsilon}. \tag{A9}$$

As before, the energy balance is written as

$$\frac{\partial}{\partial t}\langle n_e\epsilon\rangle_{inter}=S_{inter}(t)=A\int_0^{\epsilon_c}\left(\frac{\partial f(\epsilon)}{\partial t}\right)_{inter}\epsilon^{3/2}d\epsilon, \tag{A10}$$

where $S_{inter}$ is given by Eqs. (A3). Accordingly, the $K_{inter}^{+}$ parameter is expressed as

$$K_{inter}^{+}=\frac{S_{inter}/A}{\epsilon_f^{3/2}[1-f(\epsilon_f)]\left(1-\dfrac{\int_0^{\epsilon_f}\epsilon^{3/2}f(\epsilon)\,d\epsilon}{\epsilon_f\int_0^{\epsilon_f}\sqrt{\epsilon}f(\epsilon)\,d\epsilon}\right)}, \tag{A11}$$

and the operator describing interband absorption is completely defined.


[1] H. Inouye, K. Tanaka, I. Tanahashi, and K. Hirao, Phys. Rev. B **57**, 11334 (1998).
[2] S. Link and M.A. El-Sayed, J. Phys. Chem. B **103**, 8410 (1999).
[3] T.V. Shahbazyan, I.E. Perakis, and J.-Y. Bigot, Phys. Rev. Lett. **81**, 3120 (1998).
[4] C.K. Sun, F. Vallée, L.H. Acioli, E.P. Ippen, and J.G. Fujimoto, Phys. Rev. B **50**, 15337 (1994).
[5] C. Voisin, N. Del Fatti, D. Christofilos and F. Vallée, J. Phys. Chem. B **105**, 2264 (2001).
[6] S. Papernov and A.W. Schmid, Proc. SPIE **4347**, 146 (2001).
[7] S. Papernov and A.W. Schmid, J. Appl. Phys. **92**, 5720 (2002).
[8] F. Bonneau, P. Combis, J.L. Rullier, J. Vierne, H. Ward, M. Pellin, M. Savina, M. Broyer, E. Cottancin, J. Tuaillon, M. Pellarin, L. Gallais, J.Y. Nattoli, M. Perra, H. Bercegol, L. Lamaignère, M. Loiseau, and J.T. Donohue, Appl. Phys. B: Lasers Opt. **75**, 803 (2002).
[9] G. Mie, Ann. Phys. (N.Y.) **25**, 377 (1908).
[10] R. F. Harrington, *Time Harmonic Electromagnetic Fields*, Electrical and Electronic Engineering Series (McGraw-Hill, New York, 1961).
[11] P. Grua and H. Bercegol, Proc. SPIE **4347**, 579 (2001).
[12] N. Del Fatti, C. Voisin, M. Acherman, S. Tzortzakis, D. Christofilos, and F. Vallée, Phys. Rev. B **61**, 16 956 (2000).
[13] X.Y. Wang, D.M. Riffe, Y.S. Lee, and M.C. Downer, Phys. Rev. B **50**, 8016 (1994).
[14] J. L. Delcroix and A. Bers, *Physique des plasmas* (InterEditions/CNRS Editions, 1994).
[15] A. Sommerfeld, *Thermodynamics and Statistical Mechanics* (Academic Press, New York, 1964).
[16] N. W. Ashcroft and N. D. Mermin, *Solid State Physics* (Harcourt College Editions, New York, 1976).
[17] A.V. Lugovskoy and I. Bray, Phys. Rev. B **60**, 3279 (1999).
[18] L. Landau and E. Lifchitz, *Electrodynamics of Continuous Media* (Pergamon, Oxford, 1960).
[19] C. Voisin, D. Christofilos, N. Del Fatti, F. Vallée, B. Prével, E. Cottancin, J. Lerm, and M. Broyer, Phys. Rev. Lett. **85**, 2200 (2000).
[20] J.-Y. Bigot, J.-C. Merle, O. Cregut, and A. Daunois, Phys. Rev. Lett. **75**, 4702 (1995).
[21] U. Kreibig and M. Vollmer, *Optical Properties of Metal Clusters* (Springer-Verlag, Berlin, 1995).
[22] *CRC Handbook of Chemistry and Physics*, 74th ed. (CRC Press, London, 1993).
[23] W.S. Fann, R. Storz, H.W.K. Tom, and J. Bokor, Phys. Rev. B **46**, 13592 (1992).
[24] N.E. Christensen and B.O. Seraphin, Phys. Rev. B **4**, 3321 (1971).
[25] E. Spenke, *Les Semiconducteurs Électroniques* (Dunod, Paris, 1959).
[26] D.L. Griscom, J. Non-Cryst. Solids **24**, 155 (1977).
[27] D. J DiMaria, M.V. Fischetti, J. Batey, L. Dori, E. Tierney, and J. Stasiak, Phys. Rev. Lett. **57**, 3213 (1986).
[28] P. Martin, S. Guizard, Ph. Daguzan, G. Petite, P. D'Oliveira, P. Meynadier, and M. Perdrix, Phys. Rev. B **55**, 5799 (1997).
[29] R.H.M. Groneveld, R. Sprik, and A. Lagendijk, Phys. Rev. B **51**, 11 433 (1995).
[30] D.W. Snoke, W.W. Rühle, Y.C. Lu, and E. Bauser, Phys. Rev. B **45**, 10 979 (1992).
[31] P. Grua (to be published).
[32] P. Audebert, Ph. Daguzan, A. Dos Santos, J.C. Gauthier, J.P. Geindre, S. Guizard, G. Hamoniaux, K. Kraster, P. Martin, G. Petite, and A. Antonetti, Phys. Rev. Lett. **73**, 1990 (1994).
[33] N. Itoh, T. Shimizu-Iwayama and T. Fujita, J. Non-Cryst. Solids **179**, 194 (1994).
[34] N. Itoh and A. M. Stoneham, *Materials Modification by Electronic Excitation* (Cambridge University Press, Cambridge, 2000).
[35] N. Itoh, Nucl. Instrum. Methods Phys. Res. B **116**, 33 (1996).
[36] P.G. Reinhard and E. Suraud, Laser Phys. **11**, 566 (2001).